

Impurity effect and vortex cluster phase in mesoscopic type-1.5 superconductors

Tian-Yi Han¹, Guo Wang¹, Jie Li¹ and Hai Huang^{2*}

¹ School of Nuclear Science and Engineering, North China Electric Power University, Beijing, 102206, P. R. China

² Department of Mathematics and Physics, North China Electric Power University, Beijing, 102206, P. R. China

★ huanghai@ncepu.edu.cn

Abstract

Based on two-band time-dependent Ginzburg-Landau theory, we study the electromagnetic properties of two-band mesoscopic superconductors. We perform the numerical simulations with the finite element method, and determine the minimum sample size L_c for the existence of the type-1.5 superconductivity from the obtained phase diagram in the absence of impurity. Meanwhile in the presence of an isotropic impurity, our numerical results reveal that the vortex cluster state induced by the attractive defect potential will gradually appear in the mesoscopic system with the sample size $L < L_c$, and the critical defect strength is about 0.2 in the T_c disorder model. In addition, we also investigate the effect of anisotropic defect structures and multiple correlated disorders on the patterns of magnetic vortex distributions. Our theoretical study thus indicates that the diversity of impurity depositions has a significant influence on the semi-Meissner state in mesoscopic type-1.5 superconductors.

Copyright attribution to authors.

This work is a submission to SciPost Physics.

License information to appear upon publication.

Publication information to appear upon publication.

Received Date

Accepted Date

Published Date

1

Contents

1	Introduction	2
2	Model and formalism	3
3	Finite element method and numerical computations	4
4	Results and discussions	6
5	4.1 $L - \kappa_1$ phase diagram in the clean limit	6
6	4.2 Effect of an isotropic impurity in the T_c and l disorder models	8
7	4.3 Vortex cluster phase in the presence of an anisotropic impurity	11
8	4.4 Uncorrelated and correlated disorder systems	13
9	Conclusion	14
10	A Zero electric potential gauge and boundary conditions	15

13	B Discussion on convergence and relaxation time in numerical simulations	19
14	References	20

17 1 Introduction

18 Over the past two decades, two-band superconductivity has become an important research
 19 subject in condensed matter physics. This field started from the discovery of superconductivity
 20 in MgB₂ [1], where the existence of two distinct superconducting gaps reveals the complexity
 21 of Fermi surface topology in this system. Since then, extensive theoretical and experimental
 22 studies have been performed to provide novel insights into unconventional superconducting
 23 pairing mechanisms and physical properties in these materials. For example, the multi-gap
 24 superconductivity signals a new pathway to achieve more superconducting pairing modes,
 25 which can induce phase competition or coexistence between multiple bands by adjusting the
 26 external magnetic field or impurity distribution. Furthermore, the magnetic vortex behavior
 27 can be optimized through rational design of multi-band structures and its interaction with
 28 impurities can improve the overall performance of superconducting devices [2, 3].

29 As we know, each condensate in two-band superconductors is predicted to support vortex
 30 excitation with fractional quantum flux [4]. Due to the interband Josephson coupling, the
 31 vortices from different condensates are bounded together with the string interaction and their
 32 normal cores will be locked to form a composite vortex with the standard integer quantum
 33 flux in the ground state. Recently in a series of experiments of iron-based superconductors,
 34 the fractional vortices with a magnitude that varies continuously with temperature have been
 35 clearly observed in some special locations [5–7]. In general, the physics of composite vortices
 36 in the two-band system will be influenced by the coherence lengths ξ_1 and ξ_2 as well as the
 37 magnetic field penetration depth λ . When the particular condition $\xi_1 < \sqrt{2}\lambda < \xi_2$ is satisfied,
 38 there may exhibit a new superconducting state that combines characteristics of both type-1
 39 and type-2 superconductors. This so-called semi-Meissner phase or vortex cluster phase is
 40 formed due to the interaction of long-range attraction and short-range repulsion between
 41 composite vortex excitations [8–10]. The existence of this novel vortex pattern was first vi-
 42 sualized by Bitter decorations on high quality MgB₂ single crystal in 2009 [11]. Thereafter,
 43 zero-field muon spin experiments have also revealed the presence of this type-1.5 supercon-
 44 ducting state in unconventional superconductors Sr₂RuO₄ [12, 13] and LaPt₃Si [14, 15].

45 In the present paper, we study the electromagnetic effect of type-1.5 superconductors
 46 based on the time-dependent Ginzburg-Landau (TDGL) theory. With the COMSOL Multi-
 47 physics software and the finite element method, we first obtain the $L - \kappa_1$ phase diagram of
 48 the two-band superconductor in the absence of impurity, with L the sample size and κ_1 the
 49 GL parameter. Our numerical results demonstrate that there exists a critical sample size L_c
 50 for this two-band system, and the semi-Meissner state induced by long-range vortex attrac-
 51 tion disappears below L_c . Then in the presence of an isotropic impurity, we show the $g - \kappa_1$
 52 phase diagram with the sample size below L_c , where g represents the disorder strength in this
 53 system. For $|g| > 0.22$, we can directly observe the crossover of this mesoscopic system from
 54 the diamagnetic Meissner state to the vortex cluster phase, and ultimately to the Abrikosov
 55 lattice phase. Furthermore, we also discuss the possible patterns of vortex cluster induced by
 56 the anisotropic defect structures and multiple correlated disorders in this superconductor. All
 57 of our theoretical results indicate that the diversity of impurity depositions has a significant
 58 influence on the collective behaviors of magnetic vortices in the type-1.5 superconducting

59 system.

60 The rest of this article is organized as follows. In Section 2, we introduce the two-band
61 TDGL theory and apply this formalism to the type-1.5 superconductors. In Section 3, we give
62 the procedure of numerical simulations based on the finite element method. Then in Section
63 4, we systematically investigate the impurity effect and vortex cluster phase in the mesoscopic
64 system. Finally, Section 5 gives the conclusion of the paper.

65 2 Model and formalism

66 The simplest GL free energy functional of two-gap superconductors can be written as [16–20]
67

$$F = \sum_i \left[\frac{1}{2m_i} \left| \left(-i\hbar\nabla - \frac{2e}{c}\mathbf{A} \right) \Psi_i \right|^2 - \alpha_i |\Psi_i|^2 + \frac{\beta_i}{2} |\Psi_i|^4 \right] + \frac{\mathbf{B}^2}{8\pi}. \quad (1)$$

68 Here Ψ_i ($i = 1, 2$) represents the superconducting order parameter and m_i is the effective
69 mass for each band. The coefficient α_i is a function of temperature, while β_i is independent
70 of temperature. $\mathbf{B} = \nabla \times \mathbf{A}$ is the magnetic field and \mathbf{A} is the vector potential. Starting from the
71 seminal works of Thuneberg [21, 22], two main disorder models have been proposed to de-
72 scribe the effect of nonmagnetic impurities on the superconducting system in the framework
73 of the GL theory [23, 24]. The first one is the T_c disorder model with T_c the critical temper-
74 ature, which is characterized by altering the GL free energy coefficient $\alpha_i \rightarrow \alpha_{i0}g(\mathbf{r})$ in Eq.
75 (1) [25]. The other one is the l disorder model with l the mean free path, achieved by mod-
76 ifying the effective mass $1/m_i \rightarrow (1/m_i)h(\mathbf{r})$ in Eq. (1), where $h(\mathbf{r}) = l/l_m < 1$ represents
77 the ratio of the mean free path inside and outside the well-defined pinning area [26].

78 If the superconductor is driven out of equilibrium, the order parameter should relax back
79 to its equilibrium value. It is well known that this deviation of superconducting materials
80 can be conveniently described by the TDGL theories. The single-band TDGL equations were
81 first proposed by Schmid [27] and derived from the microscopic BCS theory by Gor'kov and
82 Éliashberg [28]. The extension of TDGL equations to the multi-component superconducting
83 system can be written as [29–32]

$$-\Gamma_i \frac{\partial \Psi_i}{\partial t} = \frac{\delta F}{\delta \Psi_i^*} \quad \text{and} \quad -\sigma_n \frac{\partial \mathbf{A}}{\partial t} = \frac{\delta F}{\delta \mathbf{A}} \quad (2)$$

84 where Γ_i is the relaxation time of order parameters and σ_n represents the electrical conduc-
85 tivity of the normal sample in the two-band case. Therefore, minimization of the free energy
86 F with respect to Ψ_i and \mathbf{A} leads to the following dimensionless TDGL equations in the zero-
87 electrostatic potential gauge

$$-\Gamma_1 \frac{\partial \Psi_1}{\partial t} = - \left[g(\mathbf{r}) - |\Psi_1|^2 \right] \Psi_1 + h(\mathbf{r}) (-i\nabla - \mathbf{A})^2 \Psi_1, \quad (3)$$

$$-\Gamma_2 \frac{\partial \Psi_2}{\partial t} = - \left[\frac{\alpha_{20}}{\alpha_{10}} g(\mathbf{r}) - \frac{\beta_2}{\beta_1} |\Psi_2|^2 \right] \Psi_2 + \frac{m_1}{m_2} h(\mathbf{r}) (-i\nabla - \mathbf{A})^2 \Psi_2 \quad (4)$$

89 and

$$-\frac{\partial \mathbf{A}}{\partial t} = \kappa_1^2 \nabla \times \nabla \times \mathbf{A} - \mathbf{J}_s \quad (5)$$

90 with the supercurrent

$$\mathbf{J}_s = h(\mathbf{r}) \left\{ \left[\frac{i}{2} (\Psi_1 \nabla \Psi_1^* - \Psi_1^* \nabla \Psi_1) - |\Psi_1|^2 \mathbf{A} \right] + \frac{m_1}{m_2} \left[\frac{i}{2} (\Psi_2 \nabla \Psi_2^* - \Psi_2^* \nabla \Psi_2) - |\Psi_2|^2 \mathbf{A} \right] \right\}. \quad (6)$$

Here in the clean limit with the impurity function $g = h = 1$, we at first introduce the coherence length $\xi_i^2 = \hbar^2/(2m_i\alpha_{i0})$, the London penetration depth $\lambda^{-2} = \lambda_1^{-2} + \lambda_2^{-2}$ with $\lambda_i^{-2} = 4\pi e^2\Psi_{i0}^2/(m_i c^2)$ and $\Psi_{i0} = \sqrt{\alpha_{i0}/\beta_i}$, and the GL parameter $\kappa_1 = \lambda_1/\xi_1$. We then take the coordinate \mathbf{r} in units of ξ_1 , the time t in units of $t_0 = m_1\sigma_n/(4e^2\Psi_{10}^2)$, Γ_i in units of $\alpha_{10}t_0$ and the order parameter Ψ_i in units of Ψ_{10} . We also set the magnetic field \mathbf{B} in units of $H_0 = \Phi_0/(2\pi\xi_1^2)$ with the flux quantum $\Phi_0 = \pi\hbar c/e$ and the vector potential \mathbf{A} in units of $A_0 = H_0\xi_1$.

Following Ref. [8], multi-component systems allow a type of superconductivity that is distinct from type-1 or type-2 superconductor. With the condition $\xi_1 < \sqrt{2}\lambda < \xi_2$, the type-1.5 superconducting state will originate from a peculiar vortex interaction which exhibits short-range repulsion and long-range attraction characteristics. The short-range repulsion prevents adjacent vortices from overlapping, while the long-range attraction facilitates the clustering of composite vortices. Consequently, this state is different from type-1 superconductors that completely repel magnetic flux and type-2 superconductors which allow considerable magnetic flux penetration and the formation of vortex lattice. In the ideal sample, the constraint mentioned above can be specifically expressed as

$$\sqrt{\frac{1}{2} \left(1 + \frac{m_1}{m_2} \frac{\alpha_{20}}{\alpha_{10}} \frac{\beta_1}{\beta_2} \right)} < \kappa_1 < \sqrt{\frac{1}{2} \left[\frac{m_1}{m_2} \frac{\alpha_{10}}{\alpha_{20}} + \left(\frac{m_1}{m_2} \right)^2 \frac{\beta_1}{\beta_2} \right]}. \quad (7)$$

In this circumstance, the magnetic composite vortices will form vortex clusters and coexist with domains of the two-component Meissner state in the framework of the GL theory.

In order to perform systematic numerical simulations, we need to specify appropriate boundary conditions of the superconducting sample. We use the following superconductor-insulator (or vacuum) boundary conditions in the zero-electrostatic potential gauge (see Appendix A for the detailed derivation) [33–35]

$$\nabla\Psi_i \cdot \mathbf{n} = 0, \quad \mathbf{A} \cdot \mathbf{n} = 0 \quad \text{and} \quad \nabla \times \mathbf{A} = \mathbf{H}_e \quad (8)$$

where \mathbf{n} is the outward unit vector normal to the boundary and the external applied magnetic field is set as $\mathbf{H}_e = H_e \hat{\mathbf{z}}$. The first two conditions just indicate that any current passing through the interface between a superconducting domain and vacuum/insulator would be nonphysical for each band. The third equation represents the continuity of magnetic field across the boundary. The partial differential equations (3)-(5) will be solved numerically for the mesoscopic geometry in the two-dimensional space. The initial conditions at $t = 0$ are taken as $|\Psi_i| = 1$ and $\mathbf{A} = (0, 0)$ on the xy -plane, corresponding to the Meissner state and zero magnetic field inside the superconductor.

3 Finite element method and numerical computations

Based on the COMSOL Multiphysics software platform [36], we will describe the procedure of the numerical simulations on the TDGL equations in this section. We first split the order parameters into the real and imaginary parts, i.e. $\Psi_1 = u_1 + iu_2$ and $\Psi_2 = u_3 + iu_4$. The magnetic potential is also written in component form as $\mathbf{A} = (u_5, u_6)$. In order to implement the boundary conditions, we will introduce an auxiliary variable $u_7(x, y, t)$ for reasons explained below. In the procedure of simulations, we set $\Gamma_1 = \Gamma_2 = 5$ and $m_1 = 2m_2$. To stabilize the semi-Meissner state, we also take $\alpha_{10} = \alpha_{20}$ and $\beta_1 = \beta_2$ in the calculations.

In this way, we can transform the TDGL equations into the general form of partial differ-

130 ential equations in this software package

$$\sum_k \mu_{jk} \frac{\partial u_k}{\partial t} + \sum_l \partial_l v_{jl} = \eta_j. \quad (9)$$

131 Here we have $j, k = 1, 2, \dots, 7$, $l = 1, 2$ and $(\partial_1, \partial_2) = (\partial_x, \partial_y)$. The 7×7 matrix μ_{jk} and the
132 7×2 column vector v_{jl} take the form

$$\mu_{jk} = \begin{bmatrix} 5 & 0 & 0 & 0 & 0 & 0 & 0 \\ 0 & 5 & 0 & 0 & 0 & 0 & 0 \\ 0 & 0 & 5 & 0 & 0 & 0 & 0 \\ 0 & 0 & 0 & 5 & 0 & 0 & 0 \\ 0 & 0 & 0 & 0 & 1 & 0 & 0 \\ 0 & 0 & 0 & 0 & 0 & 1 & 0 \\ 0 & 0 & 0 & 0 & 0 & 0 & 0 \end{bmatrix} \quad (10)$$

133 and

$$v_{jl} = \begin{bmatrix} -h(\mathbf{r})u_{1x} & -h(\mathbf{r})u_{1y} \\ -h(\mathbf{r})u_{2x} & -h(\mathbf{r})u_{2y} \\ -2h(\mathbf{r})u_{3x} & -2h(\mathbf{r})u_{3y} \\ -2h(\mathbf{r})u_{4x} & -2h(\mathbf{r})u_{4y} \\ 0 & \kappa_1^2 (u_{6x} - u_{5y} - H_e) \\ \kappa_1^2 (u_{5y} - u_{6x} + H_e) & 0 \\ u_5 & u_6 \end{bmatrix}. \quad (11)$$

134 Noting that the subscript x or y denotes the partial derivative with respect to the correspond-
135 ing variable here. Meanwhile, the driving force η_j contains all other terms in the TDGL
136 equations except the left handed side of Eq. (9), and detailed calculations will give all the
137 components explicitly as

$$\eta_1 = [g(\mathbf{r}) - (u_1^2 + u_2^2)] u_1 - h(\mathbf{r}) [(u_5^2 + u_6^2) u_1 - (u_{5x} + u_{6y}) u_2 - 2(u_{2x} u_5 + u_{2y} u_6)], \quad (12)$$

$$\eta_2 = [g(\mathbf{r}) - (u_1^2 + u_2^2)] u_2 - h(\mathbf{r}) [(u_5^2 + u_6^2) u_2 + (u_{5x} + u_{6y}) u_1 + 2(u_{1x} u_5 + u_{1y} u_6)], \quad (13)$$

$$\eta_3 = [g(\mathbf{r}) - (u_3^2 + u_4^2)] u_3 - 2h(\mathbf{r}) [(u_5^2 + u_6^2) u_3 - (u_{5x} + u_{6y}) u_4 - 2(u_{4x} u_5 + u_{4y} u_6)], \quad (14)$$

$$\eta_4 = [g(\mathbf{r}) - (u_3^2 + u_4^2)] u_4 - 2h(\mathbf{r}) [(u_5^2 + u_6^2) u_4 + (u_{5x} + u_{6y}) u_3 + 2(u_{3x} u_5 + u_{3y} u_6)], \quad (15)$$

$$\eta_5 = h(\mathbf{r}) [(u_{2x} u_1 - u_{1x} u_2) + 2(u_{4x} u_3 - u_{3x} u_4) - (u_1^2 + u_2^2 + 2u_3^2 + 2u_4^2) u_5], \quad (16)$$

$$\eta_6 = h(\mathbf{r}) [(u_{2y} u_1 - u_{1y} u_2) + 2(u_{4y} u_3 - u_{3y} u_4) - (u_1^2 + u_2^2 + 2u_3^2 + 2u_4^2) u_6], \quad (17)$$

$$\eta_7 = u_{5x} + u_{6y} + u_7. \quad (18)$$

138

139 Now we can examine the boundary conditions in this formalism. With the normal vector
140 $\mathbf{n} = (n_1, n_2)$ and the column vector v_{jl} , the boundary conditions in Eq. (8) can be simply

141 casted into the compact form as

$$\sum_l n_l v_{jl} = 0 \quad (19)$$

142 which is best suited to the COMSOL Multiphysics simulations. We also note that from the last
 143 equation ($j = 7$) in (9), our manipulations will give a trivial solution $u_7 = 0$ for this auxiliary
 144 variable and it insures the self-consistency of our problem.

145 COMSOL Multiphysics is a simulation platform based on the finite element method wide-
 146 ly employed in solving coupled physical problems in engineering and fundamental research.
 147 The software numerically resolves partial differential equations by discretizing the continuous
 148 computational domain into a mesh composed of finite elements [37–39]. In two-dimensional
 149 geometries, triangular elements are generally adopted due to their adaptability to irregu-
 150 lar boundaries and complex shapes. Based on this discretization, a local function space is
 151 constructed to approximate the field variables, typically using piecewise polynomial basis
 152 functions to maintain the continuity and stability across element interfaces [40]. To handle
 153 time-dependent problems with high accuracy and robustness, COMSOL utilizes implicit time-
 154 stepping schemes and often incorporates stable integration methods such as the backward
 155 Euler formulation. In our numerical calculations, we take the time step $\Delta t = 0.5t_0$ and treat
 156 a simulation as converged when the relative variations of the order parameter $|\Psi_1|$ between
 157 two sequential steps are smaller than 10^{-8} . We also set the snapshot time at $t = 10^4 t_0$, which
 158 will be justified from two perspectives in Appendix B.

159 4 Results and discussions

160 In this section, we will set the external magnetic field to $H_e = 0.8H_0$ and systematically
 161 explore the effects of sample boundary and impurities on vortex cluster excitations in the
 162 two-band superconductor.

163 4.1 $L - \kappa_1$ phase diagram in the clean limit

164 In this subsection, we first investigate the $L - \kappa_1$ phase diagram of the $L \times L$ two-band super-
 165 conductor in the absence of impurity. We perform the corresponding numerical calculations
 166 based on the TDGL theory (3)-(5). The obtained $L - \kappa_1$ phase diagram is plotted in Fig. 1.
 167 It can be seen from Fig. 1 that with the decrease of L , the vortex cluster phase produced
 168 by the long-range attractive interaction between vortices gradually vanishes. Meanwhile, we
 169 also notice the critical sample size L_c for the disappearance of this cluster state is $32\xi_1$. Thus,
 170 the superconducting system will stay in the type-1.5 regime above L_c and the type-2 regime
 171 below L_c in the absence of impurity.

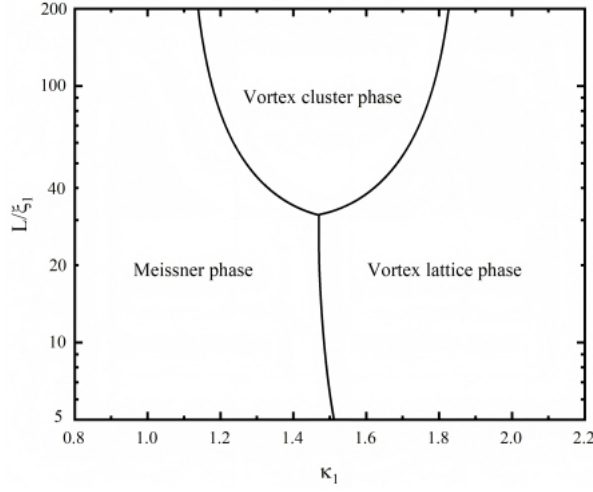


Figure 1: The $L - \kappa_1$ phase diagram of the $L \times L$ two-band superconductor in the absence of impurity. We set the external magnetic field $H_e = 0.8H_0$ in the numerical simulations, and plot the sample size L on a logarithmic scale.

As we know, the type-1.5 superconductor originates from a peculiar vortex interaction that exhibits short-range repulsion and long-range attraction characteristics. The obtained critical L_c is consistent with the characteristic length scale (about 30ξ) of the crossover from the attractive to repulsive intervortex interaction [9]. For the sample size $L > L_c$, the long-range attractive potential between vortices will dominate at the external magnetic field $H_e = 0.8H_0$ and the system is allowed to spontaneously form the stable vortex cluster. However for $L < L_c$, the repulsive intervortex interaction will prevail in the mesoscopic superconductor and the vortex cluster phase can only be induced by other effects such as impurities.

In addition to the superconducting square discussed above, we further examine the transition behaviors of mesoscopic samples with the aspect ratio different from 1 in the absence of impurity. As a simple example, we choose the $15\xi_1 \times 20\xi_1$ superconducting sample with each side length below L_c . We plot the magnetic field intensity $B_z = u_{6x} - u_{5y}$ in units of H_0 and the order parameter of the first condensate $|\Psi_1| = \sqrt{u_1^2 + u_2^2}$ in units of Ψ_{10} at $t = 10^4 t_0$ in Fig. 2. With the increase of the GL parameter κ_1 , we can see the direct transition of this system from the perfect diamagnetic state to the Abrikosov lattice phase as shown in Fig. 2. All of these numerical results thus suggest that the vortex cluster phase will be excluded for arbitrary mesoscopic sample with the characteristic scale less than L_c in the absence of impurity.

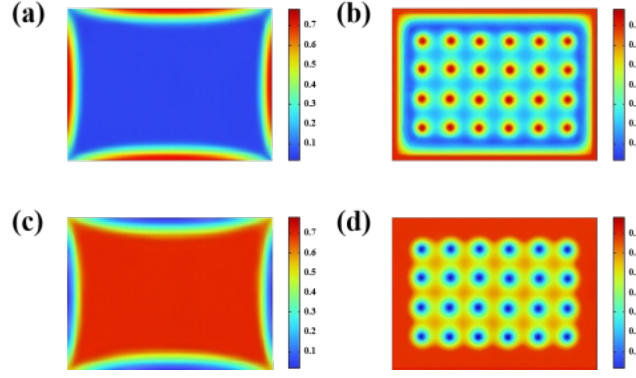


Figure 2: Transition of the magnetic field intensity B_z (a,b) and the order parameter of the first condensate $|\Psi_1|$ (c,d) for the $15\xi_1 \times 20\xi_1$ type-2 superconductor. The snapshots show the Meissner phase (a,c) and vortex lattice phase (b,d) at the GL parameter $\kappa_1 = 0.70$ and 2.10 respectively. The magnetization only has the component perpendicular to the superconducting plane.

190 4.2 Effect of an isotropic impurity in the T_c and l disorder models

191 Now, we try to explore the possible generation of the vortex cluster phase in the mesoscopic
 192 superconducting system with $L < L_c$ due to the impurity effect. As an example, we introduce
 193 an isotropic impurity with the radius $0.5\xi_1$ at the center of the $15\xi_1 \times 15\xi_1$ superconducting
 194 sample here. With the T_c disorder model, the defect function $g(\mathbf{r})$ will be characterized by
 195 the disorder strength g inside the impurity and $h(\mathbf{r}) = 1$. The obtained $g - \kappa_1$ phase diagram
 196 is shown in Fig. 3. It can be seen from Fig. 3 that with the increase of the absolute value
 197 of g , the vortex cluster phase induced by the attractive interaction from the impurity will
 198 gradually appear in the system. Meanwhile, we also see that there exists a critical impurity
 199 strength $g_c \approx -0.22$ for the generation of the vortex cluster state in this sample. Thus, the
 200 $15\xi_1 \times 15\xi_1$ mesoscopic superconductor will stay in the type-1.5 regime for $|g| > |g_c|$ in the
 201 presence of an isotropic impurity. Furthermore, it is clearly observed that for $|g| > |g_c|$, with
 202 the increase of $|g|$ the system transfers from the Meissner phase to the vortex cluster phase at
 203 a smaller critical κ_1 , and then enters the vortex lattice phase at a larger κ_1 value.

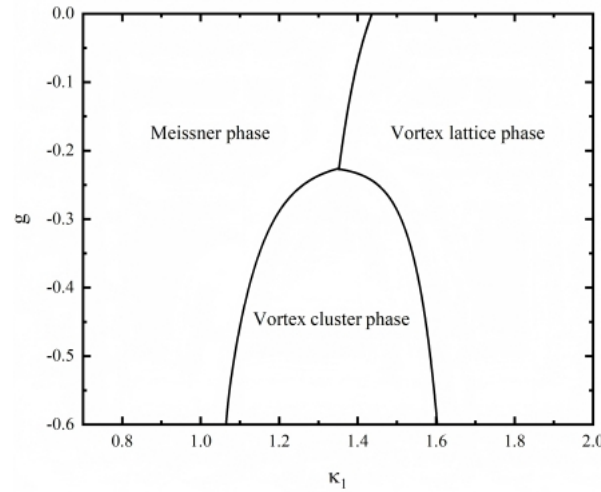


Figure 3: The $g - \kappa_1$ phase diagram of the $15\xi_1 \times 15\xi_1$ two-band superconductor in the presence of an isotropic impurity. We set the external magnetic field $H_e = 0.8H_0$ in the numerical simulations.

At this point, in order to demonstrate the robustness of vortex cluster phase induced by the localized impurity in the type-1.5 superconductor, we compare the numerical results computed from two types of disorder models, i.e., the T_c disorder model and the l disorder model. For the T_c disorder model, we choose the impurity function g to take the phenomenological form [25]

$$g(\mathbf{r}) = \begin{cases} -0.5, & \text{if } |\mathbf{r} - \mathbf{r}_0| < 0.5\xi_1 \\ 1, & \text{otherwise} \end{cases} \quad (20)$$

with $|g| > |g_c|$ inside the impurity. It is easy to see that this circular defect is centered at $\mathbf{r}_0 = (x_0, y_0)$. For simplicity, we insert this pinning site at the center of the $15\xi_1 \times 15\xi_1$ superconducting square. We plot the magnetic field intensity B_z and the order parameter of the first condensate $|\Psi_1|$ at $t = 10^4 t_0$ in Fig. 4. With the GL parameter κ_1 taken as 0.70, 1.30 and 2.10 sequentially, we can clearly observe the transitions of this type-1.5 system from the perfect diamagnetism state to the vortex cluster phase, and ultimately to the Abrikosov lattice phase. Our numerical simulations also show that the cluster phase presents the vortex pattern with octagonal symmetry and appears in the region of $1.08 < \kappa_1 < 1.58$. Moreover, it can be seen from Fig. 4(c,f) that the isotropic defect induces the localized distortion of the Abrikosov flux lattice, but will still preserve the C_4 rotational symmetry of the superconducting system.

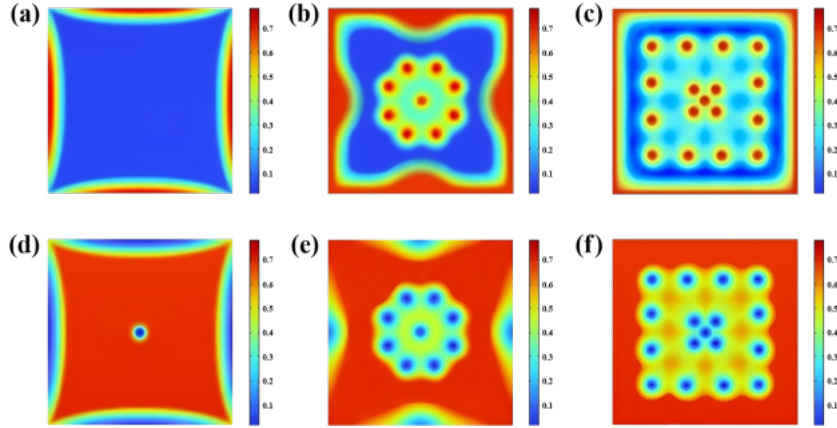


Figure 4: Transitions of the magnetic field intensity B_z (a-c) and the order parameter of the first condensate $|\Psi_1|$ (d-f) for the T_c disorder model at the presence of an isotropic defect in the $15\xi_1 \times 15\xi_1$ type-1.5 superconductor. The snapshots show the Meissner phase (a,d), vortex cluster phase (b,e) and vortex lattice phase (c,f) at the GL parameter $\kappa_1 = 0.70, 1.30$ and 2.10 respectively. The magnetization only has the component perpendicular to the superconducting plane.

For the l disorder model, we set $g(\mathbf{r}) = 1$ and the impurity function h as [26]

$$h(\mathbf{r}) = \begin{cases} 0.2, & \text{if } |\mathbf{r} - \mathbf{r}_0| < 0.5\xi_1 \\ 1, & \text{otherwise} \end{cases} \quad (21)$$

with $h < h_c$ inside the impurity. Here h_c stands for the critical disorder strength for the formation of the vortex cluster state in the l disorder model, which is estimated as 0.6 from our numerical simulations. Then, we also insert this pinning site at the center of the $15\xi_1 \times 15\xi_1$ mesoscopic sample. The magnetic field intensity B_z and the order parameter of the first condensate $|\Psi_1|$ at $t = 10^4 t_0$ are plotted in Fig. 5. For the GL parameter $\kappa_1 = 1.30$ and 2.10 , we

225 can observe a vortex cluster pattern with octagonal symmetry in Fig. 5(b,e) and the locally
 226 distorted flux lattice with C_4 rotational symmetry in Fig. 5(c,f) respectively. For this particu-
 227 lar disorder model, the vortex cluster phase is generated around the pinning site within the
 228 range $1.06 < \kappa_1 < 1.59$. Based on the numerical results mentioned above, we can conclude
 229 that within the framework of the GL theory, the T_c and l disorder models are qualitatively
 230 equivalent in describing the local effect of the impurity on collective vortex distributions for
 231 the type-1.5 superconductor.

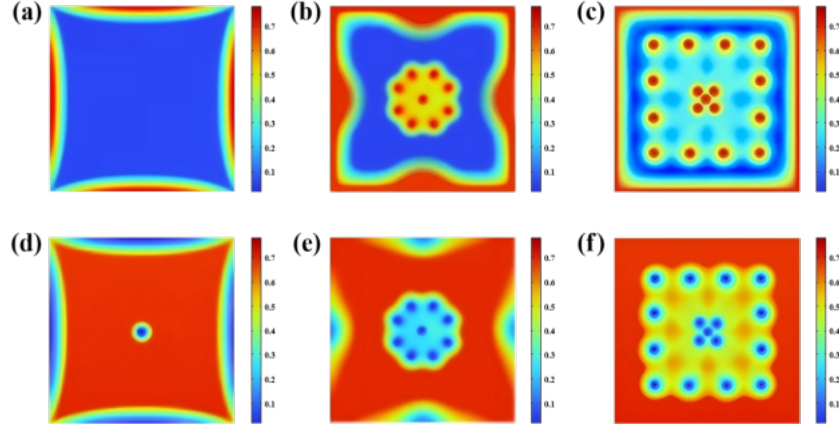


Figure 5: Transitions of the magnetic field intensity B_z (a-c) and the order parameter of the first condensate $|\Psi_1|$ (d-f) for the l disorder model at the presence of an isotropic defect in the $15\xi_1 \times 15\xi_1$ type-1.5 superconductor. The snapshots show the Meissner phase (a,d), vortex cluster phase (b,e) and vortex lattice phase (c,f) at the GL parameter $\kappa_1 = 0.70, 1.30$ and 2.10 respectively. The magnetization only has the component perpendicular to the superconducting plane.

232 At the same time, in the type-2 regime, we take the defect strength $g = -0.1$ for the T_c
 233 disorder model and $h = 0.8$ for the l disorder model inside each isotropic impurity. We still
 234 insert this pinning site at the center of the $15\xi_1 \times 15\xi_1$ superconducting square. We plot the
 235 magnetic field intensity B_z and the order parameter of the first condensate $|\Psi_1|$ at $t = 10^4 t_0$
 236 in Fig. 6 and Fig. 7. With the GL parameter κ_1 taken as 0.70 and 2.10 sequentially, we can
 237 observe the direct transition of this type-2 system from the perfect diamagnetic state to the
 238 Abrikosov lattice phase in Fig. 6 and Fig. 7. Based on the numerical calculations mentioned
 239 above, we can see that both the T_c and l disorder models give the similar results for the type-2
 240 systems.

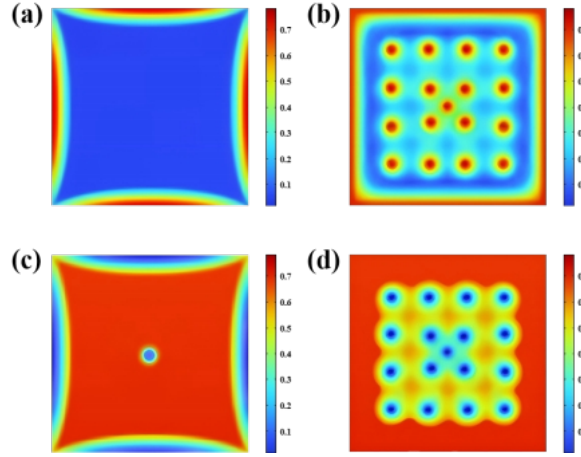


Figure 6: Transition of the magnetic field intensity B_z (a,b) and the order parameter of the first condensate $|\Psi_1|$ (c,d) for the T_c disorder model at the presence of an isotropic defect in the $15\xi_1 \times 15\xi_1$ type-2 superconductor. The snapshots show the Meissner phase (a,c) and vortex lattice phase (b,d) at the GL parameter $\kappa_1 = 0.70$ and 2.10 respectively. The magnetization only has the component perpendicular to the superconducting plane.

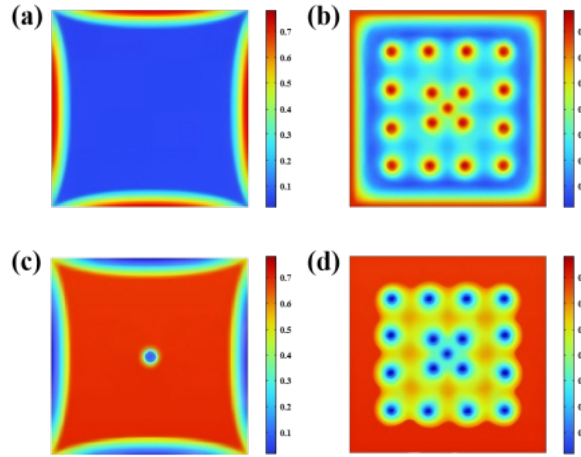


Figure 7: Transition of the magnetic field intensity B_z (a,b) and the order parameter of the first condensate $|\Psi_1|$ (c,d) for the l disorder model at the presence of an isotropic defect in the $15\xi_1 \times 15\xi_1$ type-2 superconductor. The snapshots show the Meissner phase (a,c) and vortex lattice phase (b,d) at the GL parameter $\kappa_1 = 0.70$ and 2.10 respectively. The magnetization only has the component perpendicular to the superconducting plane.

241 4.3 Vortex cluster phase in the presence of an anisotropic impurity

242 In addition to the isotropic impurity discussed above, we will investigate the effect of trian-
 243 gular and square defect configurations on the vortex cluster phase in the T_c disorder model.
 244 The triangular or square impurity is with a side length of ξ_1 and placed at the center of the
 245 $15\xi_1 \times 15\xi_1$ mesoscopic superconducting system. We also set the impurity function $g = -0.5$
 246 inside the impurity. Then, we plot the magnetic field intensity B_z and the order parameter of
 247 the first condensate $|\Psi_1|$ at $t = 10^4 t_0$ for triangular and square defect configurations in Fig. 8
 248 and Fig. 9 respectively. With the GL parameter κ_1 taken as 0.70, 1.30 and 2.10 sequentially,

we can clearly observe the transitions of this system from the perfect diamagnetism state to the vortex cluster phase, and ultimately to the vortex lattice phase. For the triangular (or square) impurity case, the peculiar vortex cluster is generated around the pinning site within the range $1.15 < \kappa_1 < 1.52$ (or $1.03 < \kappa_1 < 1.62$). It can be seen from Fig. 8(b,e) that the introduction of triangular defect breaks the C_4 rotational symmetry of the mesoscopic system and will form a distorted cluster in this circumstance. In contrast, the presence of square impurity ensures that the vortex pattern will still preserve the C_4 rotational symmetry, as shown in Figs. 9(b,e) and 9(c,f).

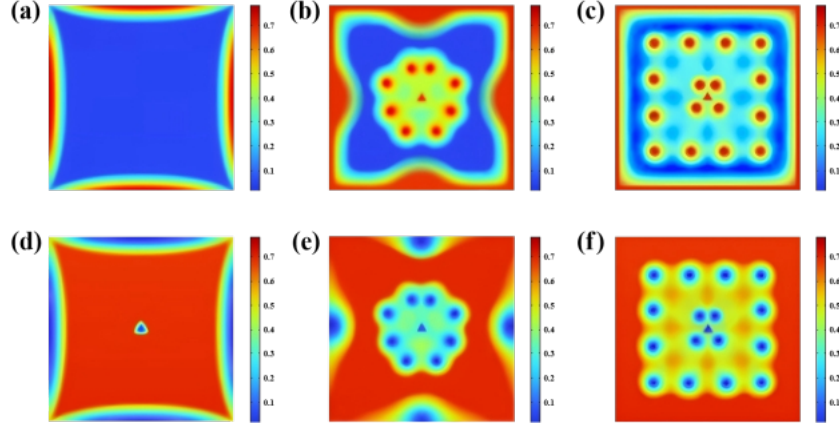


Figure 8: Transitions of the magnetic field intensity B_z (a-c) and the order parameter of the first condensate $|\Psi_1|$ (d-f) at the presence of a triangular defect in the $15\xi_1 \times 15\xi_1$ type-1.5 superconductor. The snapshots show the Meissner phase (a,d), vortex cluster phase (b,e) and vortex lattice phase (c,f) at the GL parameter $\kappa_1 = 0.70, 1.30$ and 2.10 respectively. The magnetization only has the component perpendicular to the superconducting plane.

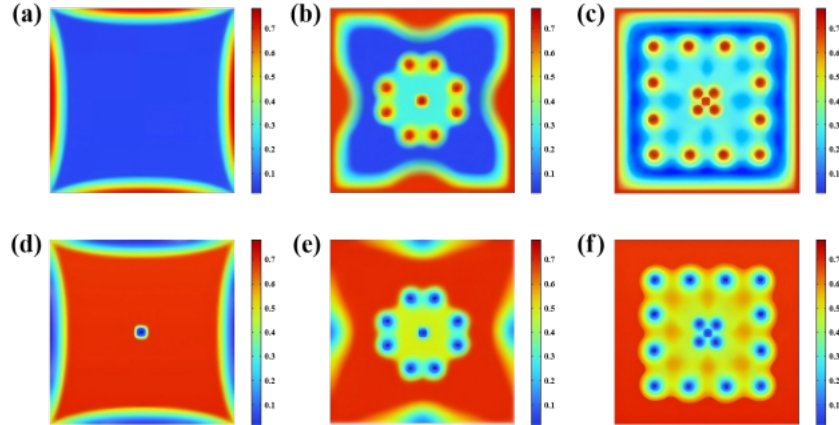


Figure 9: Transitions of the magnetic field intensity B_z (a-c) and the order parameter of the first condensate $|\Psi_1|$ (d-f) at the presence of a square defect in the $15\xi_1 \times 15\xi_1$ type-1.5 superconductor. The snapshots show the Meissner phase (a,d), vortex cluster phase (b,e) and vortex lattice phase (c,f) at the GL parameter $\kappa_1 = 0.70, 1.30$ and 2.10 respectively. The magnetization only has the component perpendicular to the superconducting plane.

257 4.4 Uncorrelated and correlated disorder systems

258 In this subsection, we set the disorder strength $|g| > |g_c|$ at the impurity sites in the T_c
 259 disorder model, and discuss the effects of multiple uncorrelated and correlated defects on
 260 vortex cluster patterns in the $15\xi_1 \times 15\xi_1$ mesoscopic superconductor. In the uncorrelated
 261 case, we choose the impurity function $g(\mathbf{r})$ to take the phenomenological form

$$g(\mathbf{r}) = \prod_{n=1}^N g_n(\mathbf{r}) \quad \text{with} \quad g_n(\mathbf{r}) = \begin{cases} -0.5, & \text{if } |\mathbf{r} - \mathbf{r}_{0n}| < 0.5\xi_1 \\ 1, & \text{otherwise} \end{cases}. \quad (22)$$

262 It is easy to see that the isotropic impurity is centered at $\mathbf{r}_{0n} = (x_{0n}, y_{0n})$ with $n = 1, 2, \dots, N$.
 263 For simplicity, we take the impurity number $N = 2$ and select the pinning centers at $(\pm 3\xi_1, 0)$
 264 in $15\xi_1 \times 15\xi_1$ superconducting sample, which ensures the uncorrelation between these two
 265 defects. We plot the magnetic field intensity B_z and the order parameter of the first condensate
 266 $|\Psi_1|$ at $t = 10^4 t_0$ in Fig. 10. Different from the single impurity case, multiple vortex clusters
 267 are generated around the pinning sites within $0.87 < \kappa_1 < 1.77$. With the GL parameter
 268 $\kappa_1 = 1.30$, we can see from Fig. 10(b,e) that each vortex cluster exhibits the identical pattern
 269 with hexagonal symmetry. Meanwhile for $\kappa_1 = 2.10$, as shown in Fig. 10(c,f), we can clearly
 270 observe the localized distortions around the pinning positions in the flux lattice due to the
 271 attraction of vortices by impurities.

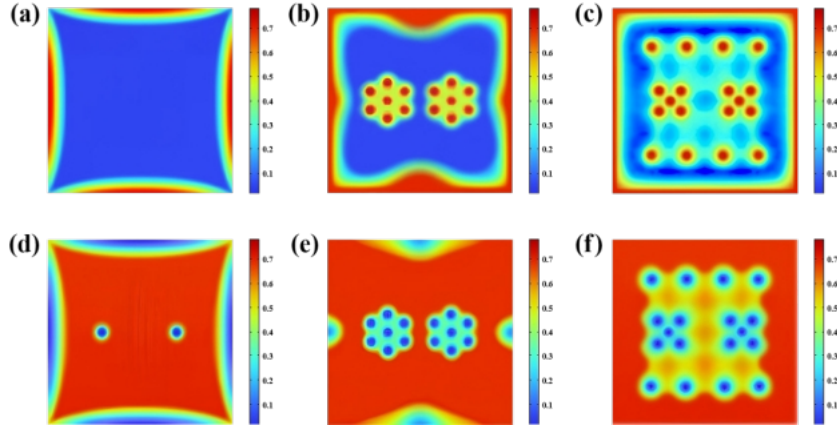


Figure 10: Transitions of the magnetic field intensity B_z (a-c) and the order parameter of the first condensate $|\Psi_1|$ (d-f) at the presence of two uncorrelated defects in the $15\xi_1 \times 15\xi_1$ type-1.5 superconductor. The snapshots show the Meissner phase (a,d), vortex cluster phase (b,e) and vortex lattice phase (c,f) at the GL parameter $\kappa_1 = 0.70, 1.30$ and 2.10 respectively. The magnetization only has the component perpendicular to the superconducting plane.

272 In order to take into account the spatial correlation between these impurities, we choose
 273 the following continuous pinning function [41, 42]

$$g(\mathbf{r}) = \prod_{n=1}^N g_n(\mathbf{r}) \quad \text{with} \quad g_n(\mathbf{r}) = \tanh\left(\frac{|\mathbf{r} - \mathbf{r}_{0n}| - R}{R_0}\right). \quad (23)$$

274 We take $R = 0.5\xi_1$ and $R_0 = 1.5\xi_1$ in Eq. (23), and then perform numerical simulations in
 275 the $15\xi_1 \times 15\xi_1$ mesoscopic superconductor. For comparison with the uncorrelated case, we
 276 still choose the defect centers at $(\pm 3\xi_1, 0)$. We plot the magnetic field intensity B_z and the

order parameter of the first condensate $|\Psi_1|$ at $t = 10^4 t_0$ in Fig. 11. Note that with this new impurity function, we can obtain the stable vortex cluster phase within $0.92 < \kappa_1 < 1.71$. For $\kappa_1 = 1.30$, it is shown in Fig. 11(b,e) that two vortex clusters induced by uncorrelated disorders in Fig. 10(b,e) are fused into a single larger cluster here. Meanwhile with $\kappa_1 = 2.10$, we can find a vortex lattice pattern with local distortions around the impurities in Fig. 11(c,f).

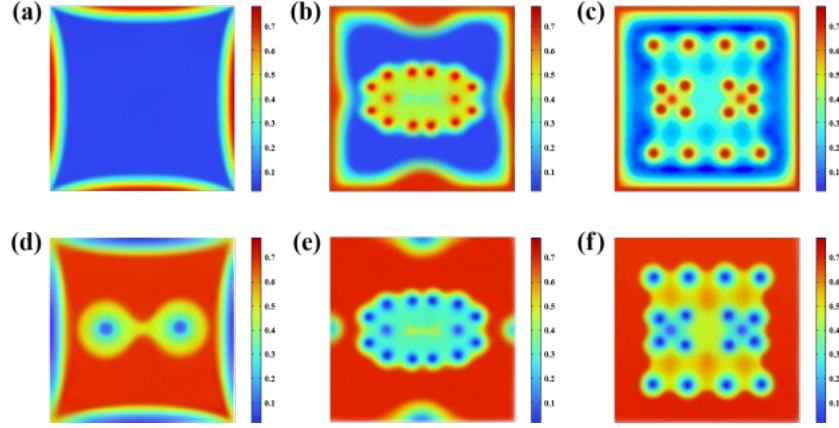


Figure 11: Transitions of the magnetic field intensity B_z (a-c) and the order parameter of the first condensate $|\Psi_1|$ (d-f) at the presence of two correlated defects in the $15\xi_1 \times 15\xi_1$ type-1.5 superconductor. The snapshots show the Meissner phase (a,d), vortex cluster phase (b,e) and vortex lattice phase (c,f) at the GL parameter $\kappa_1 = 0.70, 1.30$ and 2.10 respectively. The magnetization only has the component perpendicular to the superconducting plane.

5 Conclusion

Based on two-band TDGL theory, we explore the impurity effect on the vortex collective behaviors in the mesoscopic type-1.5 superconductor. With the finite element method, the investigations suggest that the vortex cluster phase will be excluded for arbitrary mesoscopic sample with the characteristic scale less than L_c in the absence of impurity. In the presence of an isotropic impurity, our numerical results give the direct evidence for the existence of semi-Meissner state at $|g| > |g_c|$ due to the attractive defect interaction. We also discuss the effect of anisotropic defect structures and multiple correlated disorders on the possible patterns of magnetic vortex distributions. We hope that our theoretical results will inspire further research on better understanding novel vortex dynamics and transport properties in two-band superconductors.

Acknowledgements

One of the authors (H.H.) would like to thank Prof. Z.-Z. Gan for helpful discussions. We would also like to thank the anonymous referees for very inspiring suggestions.

Author contributions Conceptualization, T.H., G.W., J.L. and H.H.; methodology, T.H., G.W., J.L. and H.H.; software, T.H., G.W.; validation, G.W., J.L. and H.H.; formal analysis, T.H., G.W., J.L. and H.H.; investigation, T.H., G.W., J.L. and H.H.; resources, H.H.; data curation, T.H., G.W., J.L. and H.H.; writing-original draft preparation, T.H., G.W. and H.H.; writing-review

and editing, T.H., G.W., J.L. and H.H.; visualization, T.H.; supervision, G.W., J.L. and H.H.; project administration, H.H. All authors have read and agreed to the published version of the manuscript.

A Zero electric potential gauge and boundary conditions

In this Appendix, we will discuss a particular gauge choice of the boundary conditions and present a microscopic derivation of the dimensionless boundary condition $(\nabla - i\mathbf{A})\Psi_i \cdot \mathbf{n} = 0$. Firstly, we try to show that in the zero electric potential gauge, the dimensionless boundary conditions will take the form

$$\nabla\Psi_i \cdot \mathbf{n} = 0, \quad \mathbf{A} \cdot \mathbf{n} = 0 \quad \text{and} \quad \nabla \times \mathbf{A} = \mathbf{H}_e \quad (\text{A.1})$$

as adopted in Eq. (8).

We start from the following gauge invariant boundary conditions between a two-band superconductor and an insulator (or vacuum)

$$(\nabla - i\mathbf{A})\Psi_i \cdot \mathbf{n} = 0, \quad \left(\frac{\partial \mathbf{A}}{\partial t} + \nabla\varphi \right) \cdot \mathbf{n} = 0 \quad \text{and} \quad \nabla \times \mathbf{A} = \mathbf{H}_e. \quad (\text{A.2})$$

Here φ is defined as the electric potential. Given an arbitrary function χ , the gauge transformation takes the form as

$$\Psi_i \rightarrow \Psi_i e^{i\chi}, \quad \mathbf{A} \rightarrow \mathbf{A} + \nabla\chi \quad \text{and} \quad \varphi \rightarrow \varphi - \frac{\partial \chi}{\partial t}. \quad (\text{A.3})$$

It is easy to show that the boundary conditions in Eq. (A.2) maintain the gauge invariance. Then with the zero electric potential gauge, we can get from the transformation in Eq. (A.3)

$$\frac{\partial \chi}{\partial t} = \varphi. \quad (\text{A.4})$$

Plugging this condition into the second equation of the boundary conditions (A.2), it leads to

$$\frac{\partial \mathbf{A}}{\partial t} \cdot \mathbf{n} = 0 \quad (\text{A.5})$$

in this new gauge. This equation can be integrated to give $\mathbf{A} \cdot \mathbf{n} = 0$, which transforms the boundary condition $(\nabla - i\mathbf{A})\Psi_i \cdot \mathbf{n} = 0$ into the form $\nabla\Psi_i \cdot \mathbf{n} = 0$. Based on the analysis above, we can see that the boundary conditions in Eq. (A.1) are simply the result of a particular gauge choice.

Secondly, we would like to give a microscopic derivation of the dimensionless boundary condition $(\nabla - i\mathbf{A})\Psi_i \cdot \mathbf{n} = 0$ which is presented in Eq. (A.2). We try to show that at the interface of two-band superconductor and insulator (or vacuum), this boundary condition is applicable not only for the simple $U(1) \times U(1)$ symmetric model studied here but also the two-component GL models in general. In this process, we will follow the procedure in the single-band case suggested by de Gennes [43].

Based on the work of Zhitomirsky and Dao [44], we write the Hamiltonian of a two-band superconductor as

$$H = \sum_{i\sigma} c_{i\sigma}^\dagger(\mathbf{r}) \hat{h}(\mathbf{r}) c_{i\sigma}(\mathbf{r}) - \sum_{ii'} g_{ii'} c_{i\uparrow}^\dagger(\mathbf{r}) c_{i\downarrow}^\dagger(\mathbf{r}) c_{i'\downarrow}(\mathbf{r}) c_{i'\uparrow}(\mathbf{r}). \quad (\text{A.6})$$

Here, $i, i' = 1, 2$ are the band indices and $\sigma = \uparrow, \downarrow$ is the spin index. $\hat{h}(\mathbf{r})$ is the single particle Hamiltonian of the normal metal, and $g_{ii'}$ are the effective electron-electron interaction constants with $g_{12} = g_{21}$.

331 We can introduce the gap functions

$$\Delta_i(\mathbf{r}) = - \sum_{i'} g_{ii'} \langle c_{i'\downarrow}(\mathbf{r}) c_{i'\uparrow}(\mathbf{r}) \rangle \quad (\text{A.7})$$

332 and transform the Hamiltonian into the mean field form

$$H_{\text{eff}} = \sum_{i\sigma} c_{i\sigma}^\dagger(\mathbf{r}) \hat{h}(\mathbf{r}) c_{i\sigma}(\mathbf{r}) + \sum_i \left[\Delta_i(\mathbf{r}) c_{i\uparrow}^\dagger(\mathbf{r}) c_{i\downarrow}^\dagger(\mathbf{r}) + \text{H.c.} \right]. \quad (\text{A.8})$$

333 This effective Hamiltonian can be diagonalized by means of the Bogoliubov transformation
334 with b and b^\dagger the annihilation and creation operators of quasi-particle excitations

$$c_{i\uparrow}(\mathbf{r}) = \sum_{\mathbf{k}} \left[u_{i\mathbf{k}}(\mathbf{r}) b_{i\mathbf{k}\uparrow} - v_{i\mathbf{k}}^*(\mathbf{r}) b_{i\mathbf{k}\downarrow}^\dagger \right] \quad (\text{A.9})$$

335 and

$$c_{i\downarrow}(\mathbf{r}) = \sum_{\mathbf{k}} \left[u_{i\mathbf{k}}(\mathbf{r}) b_{i\mathbf{k}\downarrow} + v_{i\mathbf{k}}^*(\mathbf{r}) b_{i\mathbf{k}\uparrow}^\dagger \right] \quad (\text{A.10})$$

336 where \mathbf{k} is the wave vector. With the anti-commutation relations between the fermion opera-
337 tors and the equation of motion for $c_{i\sigma}(\mathbf{r})$, we can obtain the Bogoliubov-de Gennes equations
338 for a two-band superconductor

$$\begin{pmatrix} \hat{h} & \Delta_i(\mathbf{r}) \\ \Delta_i^*(\mathbf{r}) & -\hat{h}^* \end{pmatrix} \begin{pmatrix} u_{i\mathbf{k}}(\mathbf{r}) \\ v_{i\mathbf{k}}(\mathbf{r}) \end{pmatrix} = E_{i\mathbf{k}} \begin{pmatrix} u_{i\mathbf{k}}(\mathbf{r}) \\ v_{i\mathbf{k}}(\mathbf{r}) \end{pmatrix} \quad (\text{A.11})$$

339 where $E_{i\mathbf{k}}$ is the energy of the excitation. Then with Eq. (A.7), we can transform the self-
340 consistent gap equations into

$$\Delta_i(\mathbf{r}) = \sum_{i'\mathbf{k}} g_{ii'} v_{i'\mathbf{k}}^*(\mathbf{r}) u_{i'\mathbf{k}}(\mathbf{r}) [1 - 2f(E_{i'\mathbf{k}})] \quad (\text{A.12})$$

341 with $f(E_{i\mathbf{k}}) = [1 + \exp(E_{i\mathbf{k}}/k_B T)]^{-1}$ and T the temperature.

342 In the analogy with the single-band case, for small gap functions Δ_i , we can obtain the
343 linearized form of self-consistency conditions from Eqs. (A.11) and (A.12) as

$$\Delta_i(\mathbf{r}) = \sum_{i'} \int K_{ii'}(\mathbf{r}, \mathbf{r}') \Delta_{i'}(\mathbf{r}') d\mathbf{r}' \quad (\text{A.13})$$

344 with the kernel

$$K_{ii'}(\mathbf{r}, \mathbf{r}') = \frac{g_{ii'}}{2} \sum_{\mathbf{k}\mathbf{k}'} \frac{\tanh\left(\frac{\varepsilon_{i'\mathbf{k}}}{2k_B T}\right) + \tanh\left(\frac{\varepsilon_{i'\mathbf{k}'}}{2k_B T}\right)}{\varepsilon_{i'\mathbf{k}} + \varepsilon_{i'\mathbf{k}'}} \Phi_{i'\mathbf{k}}^*(\mathbf{r}') \Phi_{i'\mathbf{k}'}^*(\mathbf{r}') \Phi_{i'\mathbf{k}}(\mathbf{r}) \Phi_{i'\mathbf{k}'}(\mathbf{r}). \quad (\text{A.14})$$

345 Here $\Phi_{i'\mathbf{k}}(\mathbf{r})$ and $\varepsilon_{i'\mathbf{k}}$ are defined as the normal-state eigenfunction and eigenvalue of the
346 electron with $\hat{h}\Phi_{i'\mathbf{k}} = \varepsilon_{i'\mathbf{k}}\Phi_{i'\mathbf{k}}$.

347 We now assume the small spatial variations in the vector potential \mathbf{A} . Then the eigenfunc-
348 tions $\Phi_{i'\mathbf{k}}$ in the normal metal in the presence of \mathbf{A} will differ from the eigenfunctions $w_{i'\mathbf{k}}$ in
349 the absence of \mathbf{A} by only a phase factor, i.e.,

$$\Phi_{i'\mathbf{k}}^*(\mathbf{r}') \Phi_{i'\mathbf{k}}(\mathbf{r}) \rightarrow w_{i'\mathbf{k}}^*(\mathbf{r}') w_{i'\mathbf{k}}(\mathbf{r}) \exp \left[\frac{i}{2} \mathbf{A} \cdot (\mathbf{r} - \mathbf{r}') \right]. \quad (\text{A.15})$$

350 Plugging into Eq. (A.13), it will lead to

$$\Delta_i(\mathbf{r}) = \sum_{i'} \int \bar{K}_{ii'}(\mathbf{r}, \mathbf{r}') \Delta_{i'}(\mathbf{r}') \exp [i\mathbf{A} \cdot (\mathbf{r} - \mathbf{r}')] d\mathbf{r}' \quad (\text{A.16})$$

351 with the kernel in the absence of external magnetic field

$$\bar{K}_{ii'}(\mathbf{r}, \mathbf{r}') = \frac{g_{ii'}}{2} \sum_{\mathbf{k}\mathbf{k}'} \frac{\tanh\left(\frac{\varepsilon_{i'\mathbf{k}}}{2k_B T}\right) + \tanh\left(\frac{\varepsilon_{i'\mathbf{k}'}}{2k_B T}\right)}{\varepsilon_{i'\mathbf{k}} + \varepsilon_{i'\mathbf{k}'}} w_{i'\mathbf{k}}^*(\mathbf{r}') w_{i'\mathbf{k}'}^*(\mathbf{r}') w_{i'\mathbf{k}}(\mathbf{r}) w_{i'\mathbf{k}'}(\mathbf{r}). \quad (\text{A.17})$$

352 Thus from Eq. (A.16), we can write

$$\Delta_i(\mathbf{r}) = \bar{\Delta}_i(\mathbf{r}) \exp(i\mathbf{A} \cdot \mathbf{r}) \quad (\text{A.18})$$

353 with $\bar{\Delta}_i(\mathbf{r})$ the superconducting gap function in the absence of \mathbf{A} . Then we have

$$\bar{\Delta}_i(\mathbf{r}) = \sum_{i'} \int \bar{K}_{ii'}(\mathbf{r}, \mathbf{r}') \bar{\Delta}_{i'}(\mathbf{r}') d\mathbf{r}'. \quad (\text{A.19})$$

354 Now, we can examine the behavior of the superconducting gap functions near the
355 superconductor-insulator interface. Following the procedure pioneered by de Gennes, we
356 suppose that the gap functions close to the surface behaves as

$$\bar{\Delta}_i(s) = \bar{\Delta}_{i0} + \left(\sum_{i'} \frac{\xi_1}{b_{ii'}} \bar{\Delta}_{i'0} \right) s. \quad (\text{A.20})$$

357 Here s measures the normal distance from the boundary in units of ξ_1 and $s > 0$ is defined
358 in the superconductor. For simplicity, we set the cross section of the boundary as 1. $\bar{\Delta}_{i0}$ rep-
359 represents the gap function at the boundary and $b_{ii'}$ denotes the intraband or interband surface
360 extrapolation length for the two-band superconductor. From Eq. (A.20), we can establish the
361 boundary condition between the two-band superconductor and the insulator (or vacuum) at
362 $s = 0$

$$\frac{d\bar{\Delta}_i}{ds} = \sum_{i'} \frac{\xi_1}{b_{ii'}} \bar{\Delta}_{i'} \quad (\text{A.21})$$

363 in the absence of external magnetic field.

364 Meanwhile, with the explicit expressions of the kernels in the bulk system and the addition
365 of nonlinear terms to the gap equations, we can obtain the two-band GL equations from Eq.
366 (A.19) as [44]

$$-\alpha_1 \bar{\Delta}_1 + \beta_1 |\bar{\Delta}_1|^2 \bar{\Delta}_1 - \gamma_1 \nabla^2 \bar{\Delta}_1 - R_{12} \bar{\Delta}_2 = 0 \quad (\text{A.22})$$

367 and

$$-\alpha_2 \bar{\Delta}_2 + \beta_2 |\bar{\Delta}_2|^2 \bar{\Delta}_2 - \gamma_2 \nabla^2 \bar{\Delta}_2 - R_{12} \bar{\Delta}_1 = 0, \quad (\text{A.23})$$

368 with the GL parameters

$$\alpha_{1,2} = N_{1,2} \left[\frac{1}{\lambda_{\max}} - \frac{\lambda_{22,11}}{\lambda} + \ln \left(\frac{T_{c0}}{T} \right) \right], \quad \beta_i = \frac{7 \zeta(3) N_i}{16 \pi^2 (k_B T_{c0})^2}, \quad (\text{A.24})$$

$$\gamma_i = \frac{7 \zeta(3) \hbar^2 N_i v_{Fi}^2}{16 \pi^2 (k_B T_{c0})^2} \quad \text{and} \quad R_{12} = \frac{N_1 \lambda_{12}}{\lambda} = \frac{N_2 \lambda_{21}}{\lambda}.$$

369 Here $\lambda_{ii'} = g_{ii'} N_{i'}$ with $N_{i'}$ the density of states at the Fermi level for each band,
370 $\lambda = \lambda_{11} \lambda_{22} - \lambda_{12} \lambda_{21}$ and $\lambda_{\max} = \frac{1}{2} \left[(\lambda_{11} + \lambda_{22}) + \sqrt{(\lambda_{11} - \lambda_{22})^2 + 4 \lambda_{12} \lambda_{21}} \right]$ the largest
371 eigenvalue of λ -matrix. T_{c0} is the bulk critical temperature and v_{Fi} is the average Fermi
372 velocity for each band.

In the spatially homogeneous case, we can neglect the gradient γ -terms. Eqs. (A.22) and (A.23) yield the gap equation at $T = T_{c0}$

$$\begin{pmatrix} \lambda_{11} & \lambda_{12} \\ \lambda_{21} & \lambda_{22} \end{pmatrix} \begin{pmatrix} \bar{\Delta}_1 \\ \bar{\Delta}_2 \end{pmatrix} = \lambda_{\max} \begin{pmatrix} \bar{\Delta}_1 \\ \bar{\Delta}_2 \end{pmatrix}, \quad (\text{A.25})$$

which obviously gives the consistent result.

Now, we try to determine the coefficients $b_{ii'}$ in Eq. (A.21) by solving the linearized gap equation (A.19) in absence of external magnetic field. If we introduce $\bar{K}_{ii'}^0(s, s')$ as the kernel of gap functions in the superconducting bulk system, we can transform Eq. (A.19) into

$$\bar{\Delta}_i(s) - \sum_{i'} \int \bar{K}_{ii'}^0(s, s') \bar{\Delta}_{i'}(s') ds' = - \sum_{i'} \int [\bar{K}_{ii'}^0(s, s') - \bar{K}_{ii'}(s, s')] \bar{\Delta}_{i'}(s') ds' \equiv - \sum_{i'} H_{ii'}(s). \quad (\text{A.26})$$

379

From Eqs. (A.22) and (A.23) with the higher order β -terms omitted, also noting that $\bar{K}_{ii'}^0(s, s') = \bar{K}_{ii'}^0(s - s')$ due to the translational symmetry, we can read out the Laplace transformation of $\bar{K}_{ii'}^0$ as

$$\bar{K}_{ii'}^0(p) = \frac{\lambda_{ii'}}{\lambda_{\max}} + \frac{\lambda_{ii'} \gamma_{i'}}{N_{i'} \xi_1^2} p^2. \quad (\text{A.27})$$

Plugging Eq. (A.27) into (A.26), we can get

$$\bar{\Delta}_i(p) - \sum_{i'} \left(\frac{\lambda_{ii'}}{\lambda_{\max}} \right) \bar{\Delta}_{i'}(p) - \sum_{i'} \left(\frac{\lambda_{ii'} \gamma_{i'}}{N_{i'} \xi_1^2} \right) p^2 \bar{\Delta}_{i'}(p) = - \sum_{i'} H_{ii'}(p). \quad (\text{A.28})$$

Here $\bar{\Delta}_i(p)$ and $H_{ii'}(p)$ are the Laplace transformations of $\bar{\Delta}_i(s)$ and $H_{ii'}(s)$ respectively. Since the first two terms of the left-handed side in Eq. (A.28) can be cancelled out according to Eq. (A.25), we then have

$$\sum_{i'} \left(\frac{\lambda_{ii'} \gamma_{i'}}{N_{i'} \xi_1^2} \right) p^2 \bar{\Delta}_{i'}(p) = \sum_{i'} H_{ii'}(p). \quad (\text{A.29})$$

We can see that both sides in Eq. (A.29) take the main contribution from the boundary region.

Notice that the Laplace transformation of the gap function in Eq. (A.20) takes the form

$$\bar{\Delta}_i(p) = \frac{\bar{\Delta}_{i0}}{p} + \sum_{i'} \frac{\xi_1 \bar{\Delta}_{i'0}}{b_{ii'} p^2}. \quad (\text{A.30})$$

Then at $p \rightarrow 0$, we will obtain from Eq. (A.29)

$$\sum_{i' i''} \left(\frac{\lambda_{ii'} \gamma_{i'}}{N_{i'} \xi_1 b_{ii''}} \right) \bar{\Delta}_{i''0} = \sum_{i'} H_{ii'}(p=0). \quad (\text{A.31})$$

Parallel to de Gennes' analysis, we have the sum rules

$$\int \bar{K}_{ii'}^0(s, s') ds' = \frac{\lambda_{ii'}}{\lambda_{\max}} \quad \text{and} \quad \int \bar{K}_{ii'}(s, s') ds' = \frac{\lambda_{ii'} N_{i'}(s)}{\lambda_{\max} N_{i'}} \quad (\text{A.32})$$

with $N_{i'}(s)$ the local density of states at the Fermi surface, Then, we can write the Laplace transformation of the kernel difference at $p \rightarrow 0$

$$H_{ii'}(p=0) = \int H_{ii'}(s) ds = \frac{\lambda_{ii'} \bar{\Delta}_{i'0}}{\lambda_{\max}} \int \frac{\bar{\Delta}_{i'}(s)}{\bar{\Delta}_{i'0}} \left[1 - \frac{N_{i'}(s)}{N_{i'}} \right] ds. \quad (\text{A.33})$$

Now we suppose $\bar{\Delta}_{i'}(s)/\bar{\Delta}_{i'0}$ approaches zero in the insulating region and is of the order of 1 in the metallic region. $N_{i'}(s)/N_{i'}$ also passes from $0 \rightarrow 1$ in a few interatomic distances from the boundary. Therefore, the integrand in Eq. (A.33) is nonvanishing only in a width of order of the lattice constant a . We can then estimate $H_{ii'}(p=0)$ as

$$H_{ii'}(p=0) = \frac{\lambda_{ii'}a}{\lambda_{\max}\xi_1} \bar{\Delta}_{i'0}. \quad (\text{A.34})$$

Comparing Eq. (A.31) with Eq. (A.34), we can finally obtain

$$\frac{1}{b_{ii}} = \frac{N_i a}{\gamma_i \lambda_{\max}} \quad \text{and} \quad \frac{1}{b_{12}} = \frac{1}{b_{21}} = 0. \quad (\text{A.35})$$

At this stage, we would like to point out that $1/b_{ii'} = 0$ ($i \neq i'$) is only an approximation and will become nonzero in the higher-order calculation. Even for a contact between a superconductor and an insulator, the Cooper pairs can still diffuse into the insulating region with some probability. Algebraically, this means that the gap function $\bar{\Delta}_{i'}(s)$ will also extend into the $s < 0$ region, and we can roughly estimate $\bar{\Delta}_{i'}(s) \sim \sum_{i''} T_{i'i''} \bar{\Delta}_{i''0} e^{\xi_1 s/a}$ ($s < 0$) with $T_{i'i''}$ the element of the transmission matrix at the boundary. Including the $s < 0$ part in the integration of Eq. (A.33) and noting $N_{i'}(s)/N_{i'} \approx 0$ in this region, we can get $H_{ii'}(p=0) = (\lambda_{ii'}a/\lambda_{\max}\xi_1) (\bar{\Delta}_{i'0} + \sum_{i''} T_{i'i''} \bar{\Delta}_{i''0})$. Plugging into Eq. (A.31), the coefficients of boundary terms are given by

$$\frac{1}{b_{ii}} = \frac{N_i a}{\gamma_i \lambda_{\max}} (1 + T_{ii}), \quad \frac{1}{b_{12}} = \frac{N_1 a}{\gamma_1 \lambda_{\max}} T_{12} \quad \text{and} \quad \frac{1}{b_{21}} = \frac{N_2 a}{\gamma_2 \lambda_{\max}} T_{21}. \quad (\text{A.36})$$

With the transmission coefficient from the superconductor to the insulator $T_{ii'} \ll 1$, we can obviously see that Eq. (A.35) is a good approximation.

For a typical two-band superconductor, we can estimate $\gamma_i \lambda_{\max}/N_i \sim \xi_1^2$ with $\xi_1 \sim 10^{-4}$ cm and the lattice constant $a \sim 10^{-8}$ cm, which will give $b_{ii} \sim 1$ cm. Therefore for a boundary separating a two-band superconductor from an insulator we can set $\xi_1/b_{ii'} \approx 0$. This leads to the boundary condition $d\bar{\Delta}_i/ds = 0$ from Eq. (A.21). For an arbitrary superconducting domain and in the presence of the magnetic field, we can generalize this result to $(\nabla - i\mathbf{A})\Delta_i \cdot \mathbf{n} = 0$ according to Eq. (A.18). With the phenomenological superconducting order parameter $\Psi_i \propto \Delta_i$, we can finally write down the boundary condition $(\nabla - i\mathbf{A})\Psi_i \cdot \mathbf{n} = 0$ for the interface of two-band superconductor and insulator.

B Discussion on convergence and relaxation time in numerical simulations

In this Appendix, we would like to justify the choice of the snapshot time at $t = 10^4 t_0$ in our numerical simulations from two perspectives. On one hand, we take the time step $\Delta t = 0.5 t_0$ in our numerical calculations and treat a simulation as converged when the relative variation of the order parameter $|\Psi_1|$ between two sequential steps is smaller than 10^{-8} . Our computational results indicate that for the $15\xi_1 \times 15\xi_1$ superconducting systems with different defect configurations, the system will consistently reach the convergence before the snapshot time $10^4 t_0$. On the other hand, we can define an average velocity $\bar{v} = \sum_{\delta=1}^M |\mathbf{r}_{\delta}(t + \Delta t) - \mathbf{r}_{\delta}(t)| / (M\Delta t)$ for the vortices in the system, where $\mathbf{r}_{\delta} = (x_{\delta}, y_{\delta})$ with $\delta = 1, 2, \dots, M$ stands for the instantaneous position of each vortex core. As an example, we discuss the $15\xi_1 \times 15\xi_1$ mesoscopic sample in the presence of an isotropic impurity with the disorder strength $g = -0.5$ here. In the procedure of simulations, we notice that

the vortex number in the sample will no longer change beyond $t \approx 10^3 t_0$. We then plot the variations of \bar{v} with t for the vortex cluster state and the vortex lattice phase in Fig. 12. It can be seen from Fig. 12 that the \bar{v} evolves with t and eventually stabilizes at $t < 10^4 t_0$. Therefore, it is justified for us to take the snapshots at $t = 10^4 t_0$ to present the stable vortex dynamics.

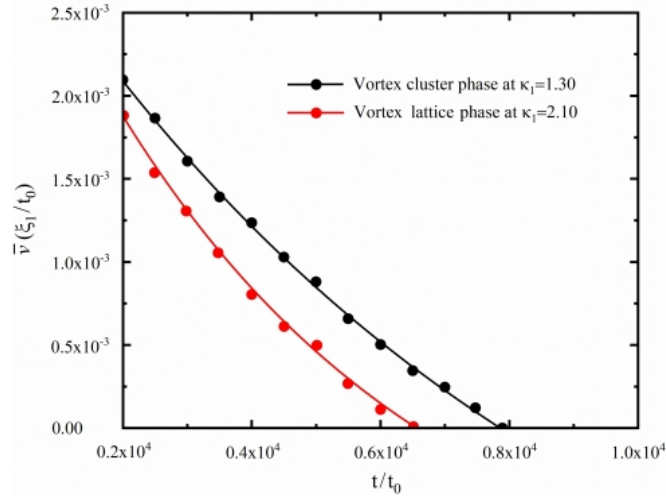


Figure 12: Variations of the average velocity \bar{v} with time t at the presence of an isotropic defect with the radius $0.5\xi_1$ in the $15\xi_1 \times 15\xi_1$ type-1.5 superconductor. We set the external magnetic field $H_e = 0.8H_0$ in the numerical simulations.

References

- [1] J. Nagamatsu, N. Nakagawa, T. Muranaka, Y. Zenitani and J. Akimitsu, *Superconductivity at 39 K in magnesium diboride*, Nature **410**, 63 (2001), doi:[10.1038/35065039](https://doi.org/10.1038/35065039).
- [2] M. Zehetmayer, *A review of two-band superconductivity: materials and effects on the thermodynamic and reversible mixed-state properties*, Supercond. Sci. Technol. **26**, 043001 (2013), doi:[10.1088/0953-2048/26/4/043001](https://doi.org/10.1088/0953-2048/26/4/043001).
- [3] T. Salamone, H. G. Hugdal, S. H. Jacobsen and M. Amundsen, *High magnetic field superconductivity in a two-band superconductor*, Phys. Rev. B **107**, 174516 (2023), doi:[10.1103/PhysRevB.107.174516](https://doi.org/10.1103/PhysRevB.107.174516).
- [4] E. Babaev, *Vortices with fractional flux in two-gap superconductors and in extended Faddeev model*, Phys. Rev. Lett. **89**, 067001 (2002), doi:[10.1103/PhysRevLett.89.067001](https://doi.org/10.1103/PhysRevLett.89.067001).
- [5] Y. Iguchi, R. A. Shi, K. Kihou, C. H. Lee, M. Barkman, A. L. Benfenati, V. Grinenko, E. Babaev and K. A. Moler, *Superconducting vortices carrying a temperature-dependent fraction of the flux quantum*, Science **380**, 1244 (2023), doi:[10.1126/science.abp9979](https://doi.org/10.1126/science.abp9979).
- [6] Q. Z. Zhou, B. R. Chen, B. K. Xiang, I. Timoshuk, J. Garaud, Y. Li, K. Y. Liang, Q. S. He, Z. J. Li, P. H. Zhang, K. Z. Yao, H. X. Yao, E. Babaev, V. Grinenko and Y. H. Wang, *Observation of single-quantum vortex splitting in the $Ba_xK_{1-x}Fe_2As_2$ superconductor*, arXiv: 2408.05902 (2024), doi:[10.48550/arXiv.2408.05902](https://doi.org/10.48550/arXiv.2408.05902).
- [7] Y. Zheng, Q. X. Hu, H. J. Ji, I. Timoshuk, H. X. Xu, Y. W. Li, Y. Gao, X. Yu, R. Wu, X. Y. Lu, V. Grinenko, E. Babaev, N. F. Q. Yuan, B. Q. Lv, C. M. Yim and H. Ding, *Direct observation*

- of quantum vortex fractionalization in multiband superconductors, arXiv: 2407.18610 (2024), doi:[10.48550/arXiv.2407.18610](https://doi.org/10.48550/arXiv.2407.18610).
- [8] E. Babaev and M. Speight, *Semi-Meissner state and neither type-I nor type-II superconductivity in multicomponent superconductors*, Phys. Rev. B **72**, 180502 (2005), doi:[10.1103/PhysRevB.72.180502](https://doi.org/10.1103/PhysRevB.72.180502).
- [9] J. Carlström, E. Babaev and M. Speight, *Type-1.5 superconductivity in multiband systems: effects of interband couplings*, Phys. Rev. B **83**, 174509 (2011), doi:[10.1103/PhysRevB.83.174509](https://doi.org/10.1103/PhysRevB.83.174509).
- [10] J. Carlström, J. Garaud and E. Babaev, *Length scales, collective modes, and type-1.5 regimes in three-band superconductors*, Phys. Rev. B **84**, 134518 (2011), doi:[10.1103/PhysRevB.84.134518](https://doi.org/10.1103/PhysRevB.84.134518).
- [11] V. Moshchalkov, M. Menghini, T. Nishio, Q. H. Chen, A. V. Silhanek, V. H. Dao, L. F. Chibotaru, N. D. Zhigadlo and J. Karpinski, *Type-1.5 superconductivity*, Phys. Rev. Lett. **102**, 117001 (2009), doi:[10.1103/PhysRevLett.102.117001](https://doi.org/10.1103/PhysRevLett.102.117001).
- [12] C. W. Hicks, J. R. Kirtley, T. M. Lippman, N. C. Koshnick, M. E. Huber, Y. Maeno, W. M. Yuhasz, M. B. Maple and K. A. Moler, *Limits on superconductivity-related magnetization in Sr_2RuO_4 and $\text{PrOs}_4\text{Sb}_{12}$ from scanning SQUID microscopy*, Phys. Rev. B **81**, 214501 (2010), doi:[10.1103/PhysRevB.81.214501](https://doi.org/10.1103/PhysRevB.81.214501).
- [13] S. J. Ray, A. S. Gibbs, S. J. Bending, P. J. Curran, E. Babaev, C. Baines, A. P. Mackenzie and S. L. Lee, *Muon-spin rotation measurements of the vortex state in Sr_2RuO_4 : type-1.5 superconductivity, vortex clustering, and a crossover from a triangular to a square vortex lattice*, Phys. Rev. B **89**, 094504 (2014), doi:[10.1103/PhysRevB.89.094504](https://doi.org/10.1103/PhysRevB.89.094504).
- [14] I. Kawasaki, I. Watanabe, H. Amitsuka, K. Kunimori, H. Tanida and Y. Onuki, *Superconducting properties of noncentrosymmetric superconductor LaPt_3Si studied by muon spin spectroscopy*, J. Phys. Soc. Jpn. **82**, 084713 (2013), doi:[10.7566/JPSJ.82.084713](https://doi.org/10.7566/JPSJ.82.084713).
- [15] T. Fujisawa, A. Yamaguchi, G. Motoyama, D. Kawakatsu, A. Sumiyama, T. Takeuchi, R. Settai and Y. Onuki, *Magnetization measurements of non-centrosymmetric superconductor LaPt_3Si : construction of low temperature magnetometers with the SQUID and Hall sensor*, Jpn. J. Appl. Phys. **54**, 048001 (2015), doi:[10.7567/JJAP.54.048001](https://doi.org/10.7567/JJAP.54.048001).
- [16] Y. S. Yerin and A. N. Omelyanchouk, *Coherent current states in a two-band superconductor*, Low Temp. Phys. **33**, 401 (2007), doi:[10.1063/1.2737547](https://doi.org/10.1063/1.2737547).
- [17] R. M. Silva, M. V. Milošević, D. Domínguez, F. M. Peeters and J. A. Aguiar, *Distinct magnetic signatures of fractional vortex configurations in multiband superconductors*, Appl. Phys. Lett. **105**, 232601 (2014), doi:[10.1063/1.4904010](https://doi.org/10.1063/1.4904010).
- [18] S. Maiti, M. Sigrist and A. Chubukov, *Spontaneous currents in a superconductor with $s + is$ symmetry*, Phys. Rev. B **91**, 161102 (2015), doi:[10.1103/PhysRevB.91.161102](https://doi.org/10.1103/PhysRevB.91.161102).
- [19] J. Garaud, M. Silaev and E. Babaev, *Thermoelectric signatures of time-reversal symmetry breaking states in multiband superconductors*, Phys. Rev. Lett. **116**, 097002 (2016), doi:[10.1103/PhysRevLett.116.097002](https://doi.org/10.1103/PhysRevLett.116.097002).
- [20] V. L. Vadimov and M. A. Silaev, *Polarization of the spontaneous magnetic field and magnetic fluctuations in $s + is$ anisotropic multiband superconductors*, Phys. Rev. B **98**, 104504 (2018), doi:[10.1103/PhysRevB.98.104504](https://doi.org/10.1103/PhysRevB.98.104504).

- [21] E. V. Thuneberg, *Elementary pinning potential in type II superconductors near H_{c2}* , J. Low Temp. Phys. **57**, 415 (1984), doi:[10.1007/BF00681201](https://doi.org/10.1007/BF00681201).
- [22] E. V. Thuneberg, *Elementary pinning potentials in superconductors with anisotropic Fermi surface*, Cryogenics **29**, 236 (1989), doi:[10.1016/0011-2275\(89\)90167-7](https://doi.org/10.1016/0011-2275(89)90167-7).
- [23] G. Blatter, M. V. Feigel'man, V. B. Geshkenbein, A. I. Larkin and V. M. Vinokur, *Vortices in high-temperature superconductors*, Rev. Mod. Phys. **66**, 1125 (1994), doi:[10.1103/RevModPhys.66.1125](https://doi.org/10.1103/RevModPhys.66.1125).
- [24] M. Friesen and P. Muzikar, *Microscopic theory of vortex pinning: impurity terms in the Ginzburg-Landau free energy*, Phys. Rev. B **53**, R11953 (1996), doi:[10.1103/PhysRevB.53.R11953](https://doi.org/10.1103/PhysRevB.53.R11953).
- [25] S. Z. Lin, S. Maiti and A. Chubukov, *Distinguishing between $s + id$ and $s + is$ pairing symmetries in multiband superconductors through spontaneous magnetization pattern induced by a defect*, Phys. Rev. B **94**, 064519 (2016), doi:[10.1103/PhysRevB.94.064519](https://doi.org/10.1103/PhysRevB.94.064519).
- [26] J. Y. Ge, J. Gutierrez, V. N. Gladilin, J. T. Devreese and V. V. Moshchalkov, *Bound vortex dipoles generated at pinning centres by Meissner current*, Nat. Commun. **6**, 6573 (2015), doi:[10.1038/ncomms7573](https://doi.org/10.1038/ncomms7573).
- [27] A. Schmid, *A time dependent Ginzburg-Landau equation and its application to the problem of resistivity in the mixed state*, Phys. Kondens. Mater. **5**, 302 (1966), doi:[10.1007/BF02422669](https://doi.org/10.1007/BF02422669).
- [28] L. P. Gor'kov and G. M. Éliashberg, *Generalization of the Ginzburg-Landau equations for non-stationary problems in the case of alloys with paramagnetic impurities*, Zh. Eksp. Teor. Fiz. **54**, 612 (1968), doi:[10.1142/9789814317344_0003](https://doi.org/10.1142/9789814317344_0003).
- [29] W. C. Gonçalves, E. Sardella, V. F. Becerra, M. V. Milošević and F. M. Peeters, *Numerical solution of the time-dependent Ginzburg-Landau equations for mixed ($d+s$)-wave superconductors*, J. Math. Phys. **55**, 041501 (2014), doi:[10.1063/1.4870874](https://doi.org/10.1063/1.4870874).
- [30] P. A. S. Mosquera, R. M. da Silva, A. Vagov, A. A. Shanenko, T. C. E. Deluque and A. J. Albino, *Nonequilibrium interband phase textures induced by vortex splitting in two-band superconductors*, Phys. Rev. B **96**, 054517 (2017), doi:[10.1103/PhysRevB.96.054517](https://doi.org/10.1103/PhysRevB.96.054517).
- [31] C. A. Aguirre, M. R. Joya and J. Barba-Ortega, *On the vortex matter in a two-band superconducting meso-prism*, Physica C **585**, 1353867 (2021), doi:[10.1016/j.physc.2021.1353867](https://doi.org/10.1016/j.physc.2021.1353867).
- [32] S. Z. Du, Y. N. Zhong, S. W. Yao, L. Peng, T. T. Shi, L. N. Sang, X. L. Liu and J. Lin, *The dynamics of current-driven vortex in two-band superconductor with $s + d$ wave pairing*, Phys. Lett. A **443**, 128206 (2022), doi:[10.1016/j.physleta.2022.128206](https://doi.org/10.1016/j.physleta.2022.128206).
- [33] S. W. Yao, L. Peng, J. Lin, J. Chen, C. B. Cai and Y. Zhou, *Properties of vortex configurations in two-band mesoscopic superconductors with Josephson coupling: the Ginzburg-Landau theory*, J. Low. Temp. Phys. **202**, 329 (2021), doi:[10.1007/s10909-020-02551-x](https://doi.org/10.1007/s10909-020-02551-x).
- [34] Y. G. Ryu, G. I. Mun, Y. N. Kwon, S. H. Kim and S. Hong, *Motion of magnetic vortices in type-II superconductor with randomly distributed pinning centers*, Physica C **602**, 1354125 (2022), doi:[10.1016/j.physc.2022.1354125](https://doi.org/10.1016/j.physc.2022.1354125).

- [35] Y. G. Ryu, J. H. Om, J. H. Kim, G. I. Ro, G. I. Mun and S. Hong, *The influence of surface defects on motion of magnetic vortices in mesoscopic type-II superconductor with randomly distributed pinning centers*, J. Supercond. Nov. Magn. **37**, 527 (2024), doi:[10.1007/s10948-024-06694-w](https://doi.org/10.1007/s10948-024-06694-w).
- [36] COMSOL, Comsol multiphysics modeling guide, (2009), <https://www.comsol.com>.
- [37] Q. Du, M. D. Gunzburger and J. S. Peterson, *Solving the Ginzburg-Landau equations by finite-element methods*, Phys. Rev. B **46**, 9027 (1992), doi:[10.1103/PhysRevB.46.9027](https://doi.org/10.1103/PhysRevB.46.9027).
- [38] T. S. Alstrøm, M. P. Sørensen, N. F. Pedersen and S. Madsen, *Magnetic flux lines in complex geometry type-II superconductors studied by the time dependent Ginzburg-Landau equation*, Acta. Appl. Math. **115**, 63 (2011), doi:[10.1007/s10440-010-9580-8](https://doi.org/10.1007/s10440-010-9580-8).
- [39] B. Oripov and S. M. Anlage, *Time-dependent Ginzburg-Landau treatment of rf magnetic vortices in superconductors: vortex semiloops in a spatially nonuniform magnetic field*, Phys. Rev. E **101**, 033306 (2020), doi:[10.1103/PhysRevE.101.033306](https://doi.org/10.1103/PhysRevE.101.033306).
- [40] J. C. Li and Y. Q. Huang, *Time-domain finite element methods for Maxwell's equations in metamaterials*, Springer Heidelberg, New York, Dordrecht London, ISBN 978-3-642-33788-8 (2013), doi:[10.1007/978-3-642-33789-5](https://doi.org/10.1007/978-3-642-33789-5).
- [41] M. P. Sørensen, N. F. Pedersen and M. Ögren, *The dynamics of magnetic vortices in type II superconductors with pinning sites studied by the time dependent Ginzburg-Landau model*, Physica C **533**, 40 (2017), doi:[10.1016/j.physc.2016.08.001](https://doi.org/10.1016/j.physc.2016.08.001).
- [42] F. M. Izrailev, A. A. Krokhin and N. M. Makarov, *Anomalous localization in low-dimensional systems with correlated disorder*, Phys. Rep. **512**, 125 (2012), doi:[10.1016/j.physrep.2011.11.002](https://doi.org/10.1016/j.physrep.2011.11.002).
- [43] P. G. de Gennes, *Superconductivity of metals and alloys*, Westview Press, New York, USA, ISBN 0-7382-0101-4 (1966), doi:[10.1201/9780429497032](https://doi.org/10.1201/9780429497032).
- [44] M. E. Zhitomirsky and V. H. Dao, *Ginzburg-Landau theory of vortices in a multigap superconductor*, Phys. Rev. B **69**, 054508 (2004), doi:[10.1103/PhysRevB.69.054508](https://doi.org/10.1103/PhysRevB.69.054508).